富山大学研究推進機構水素同位体科学研究センター研究報告35：1－12，2015.

論　文

LHDプラズマに曝したステンレス鋼の表面変質とヘリウムの吸蔵・放出

吉田直亮[1]、湯上尚之[2]、木村陽太[2]、藤原正[1]、荒木邦明[1]、吉原麗子[1]、渡邊英雄[1]、
時谷政行[3]、増崎貴[3]、波多野雄治[4]、松山政夫[4]、大矢恭久[5]、奥野健二[5]

[1]九州大学応用力学研究所、816-8580 春日市春日公園6-1
[2]九州大学大学院総合理工学研究科、816-8580 春日市春日公園6-1
[3]自然科学研究機構核融合科学研究所、509-5292 土岐市下石町322-6
[4]富山大学研究推進機構水素同位体科学研究センター、930-8555 富山市五福3190
[5]静岡大学大学院理学領域、422-8529 静岡市駿河区大谷836

Surface Properties and Retention of Helium in Stainless Steel Exposed to LHD Plasmas

N. Yoshida[1], N. Yugami[2], Y. Kimura[2], T. Fujiwara[1], K. Araki[1], R. Yoshihara[1], H. Watanabe[1], M. Tokitani[3], S. Masuzaki[3], Y. Hatano[4], M. Matsuyama[4], Y. Oya[5], K. Okuno[5]

[1] Research Institute for Applied Mechanics, Kyushu University, Kasuga-Koen, Kasuga, Fukuoka 816-8580, Japan
[2] Interdisciplinary Graduate School of Engineering Sciences, Kyushu University, Kasuga-Koen, Kasuga, Fukuoka 816-8580, Japan
[3] National Institute for Fusion Science, Oroshi, Toki, Gifu 509-5292, Japan
[4] Hydrogen Isotope Research Center, Organization for Promotion or Research, University of Toyama, Gofuku, Toyama 930-8555, Japan
[5] Faculty of Science, Shizuoka University, Ohya, Suruga-ku, Shizuoka 422-8529, Japan

(Received February 5, 2016; Accepted August 29, 2016)

Abstract

Modification of the plasma facing surface of LHD and its effects on the retention and desorption of He were examined by exposing 316L stainless steel coupons to LHD plasmas. In the erosion dominant area, formation of dense He bubbles and mixing of deposited impurities (C, O, Fe, Cr, Ni) occurred in a subsurface region of about 20 nm-thick. In the deposition

dominant area, the surface was covered by a porous carbon rich layer. Retention of He was saturated in both areas. In the erosion dominant area, He was trapped by the radiation-induced defects formed in the very thin subsurface region. The concentration of He trapped in the impurity deposition (He/C) in the deposition dominant area was estimated to be 0.9%.

1. Introduction

Large Helical Device (LHD) at National Institute for Fusion Science (NIFS) is a world-largest heliotron-type plasma confinement machine equipped with a superconducting helical coil system. Therefore, achievement of steady-state plasma discharge is one of the highest priority missions of the LHD project. Stainless steel and isotropic graphite are used in LHD for the first wall (protection plates for helical superconducting coils) and divertor plates, respectively. Usually, helium (He) has been used as the discharge gas for long-pule discharges aiming steady state operation.

Though the plasma duration time is increasing year by year, termination of the plasma has occurred often with a sudden increase in impurity radiation [1]. As pointed out by Tokitani et al., this phenomenon is attributed to certain types of plasma-wall interaction (PWI), such as arcing between the plasma and the wall, gas impurity emission and exfoliation of the deposited impurity layers [2]. Termination of long-pulse plasma occurs often not only in LHD but also in many other machines. In case of TRIAM-1M, for example, which has the world record of the discharge duration time more than 3 hours [3], control of discharge gas (hydrogen) desorption from the wall surfaces due to gradual increase of the wall temperature was a key factor to keep discharges long [4,5]. Loss of the particle balance is a common reason for the unexpected termination of long-pulse discharges.

In order to keep the particle balance, one should know influx and outflux of plasma particles through the plasma-facing surfaces of the first walls and the divertors. The plasma particle outflux, however, has been treated often as a “black box”, because the data are so limited. It depends on the properties of plasma-facing surfaces modified by many types of PWI depending on the geometrical relation with the plasma. In case of LHD, modification of the plasma-facing surfaces are various, because the internal shape of the vacuum vessel is very complicated due to the three-dimensional helical configuration. For example, thickness and microscopic structure of impurity deposition on the plasma-facing surfaces have strong poloidal and toroidal dependence [1,6]. Modification of divertor surface is also very inhomogeneous [7].

One should know the details of the thermal behavior of the discharge gas in the plasma-facing materials to understand the outflux phenomena under long-pulse discharges.

Simultaneous studies on the physical and chemical properties of the modified surfaces are also essential to understand the underlining microscopic mechanisms and to extrapolate this information to other machines.

In this paper, surface modifications in LHD due to PWI will be described at first, and then retention and desorption of He will be discussed aiming better understanding of the particle balance of He under long-pule operation.

2. Experimental procedures

Since the LHD campaign Cycle 12 (denote as C12) in 2008, several sets of metallic coupons have been regularly placed for PWI study on the surface of the inner wall near 8I and 9I ports. The positions of the coupons near 9I port are shown in Fig. 1 by numbering in the figure. In the present work, the coupons of 316L stainless steel (316LSS), material of the plasma facing wall of LHD, and those of W were used. The W coupons were employed to observe deposition of impurities including constituent elements of 316LSS (Fe, Cr and Ni). Because the inner wall of LHD is close to the main plasma and the divertor made of isotropic graphite is not so far away, PWI in this area seems stronger than that at the outer wall, in general. Surface modification of the outer wall has been reported already [2]. In LHD, He plasmas were often used for both long-pulse discharges and glow discharge cleaning. The

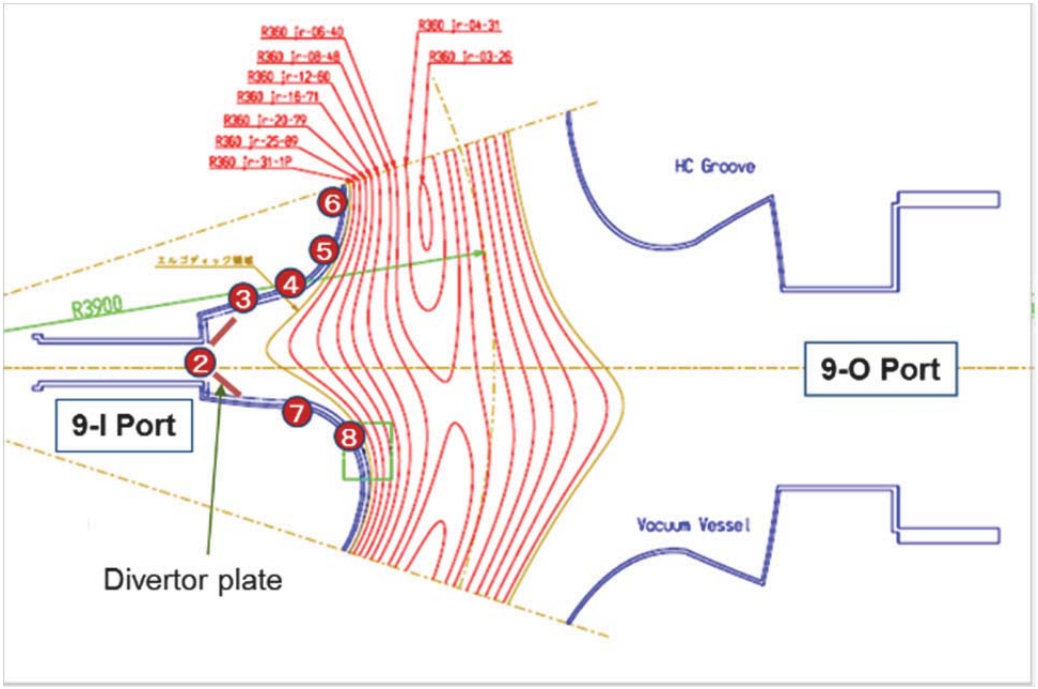

Fig. 1 Cross-sectional view of LHD at 9I port. Positions of the coupons are indicated by numbers.

temperature of the inner wall measured from the back-side using a thermocouple changed from 300 K to 310–350 K under long-pule He discharge [8].

In each experimental campaign the coupons were set before starting and taken out after finishing. Microstructure and morphology of plasma-exposed surfaces of the coupons were examined by means of transmission electron microscopy (TEM) and scanning electron microscopy (SEM). Chemical compositions were analyzed using glow discharge optical emission spectroscopy (GD-OES) and X-ray photoelectron spectroscopy (XPS). Retention of He was measured by thermal desorption spectroscopy (TDS). GD-OES analysis was carried out at University of Toyama under the framework of NIFS bilateral collaboration.

3. Experimental results and discussion

3.1 Macroscopic change of the plasma facing surfaces

Pictures of PWI-coupons placed near the 9I port at positions 3, 4 and 5 (Fig. 1) and exposed to the LHD plasmas in the campaigns C15 (2012), C16 (2013) and C17 (2014) are shown in Fig. 2. Some coupons discolored remarkably but others keep well their original metallic gloss. As described later in detail, on the dark area the impurity deposition rate exceeds the erosion rate (position 4), while on the metallic gloss area the inverse situation takes place (positions 3 and 5). In this paper, modification of the plasma-facing surfaces is discussed by classifying into two categories, deposition dominant area (DD area) and erosion dominant area (ED area).

Fig. 2 Pictures of coupons placed near 9I ports in the LHD campaigns C15, C16 and C17.

3.2 Change in microstructure

Fig. 3 shows typical TEM images of the microstructure formed in the near-surface region of the 316LSS coupons placed at 9I-3 position during the C16. Name of the coupons is noted as C16-9I-3-SS hereafter. Micrographs (a) and (b) are the top-view of the pre-thinned coupon about 50 nm-thick and the cross-sectional view, respectively. Micro-specimens for the cross-sectional observation were manufactured by using a focused ion beam (FIB) machining. As can be seen in Fig. 3 (a), very dense white dot images, which are He bubbles in nano-size [9–11], were observed near the plasma-facing surface. Large white images of 5-20 nm in diameter are well-grown He bubbles and/or dimples formed by the exfoliation of nano-blisters. Dislocation loops with black images were also formed densely. The cross-sectional view (Fig. 3 (b)) shows that the visible bubbles in nano-size are formed in the subsurface region at depths up to ~50 nm and larger ones (~10 nm in diameter) concentrate in shallower depths up to 20 nm. These are typical microstructures formed at the plasma-facing surfaces in the ED area due to He bombardment. As previously mentioned, He plasmas are often used for both long-pulse discharges and glow discharge cleaning in LHD.

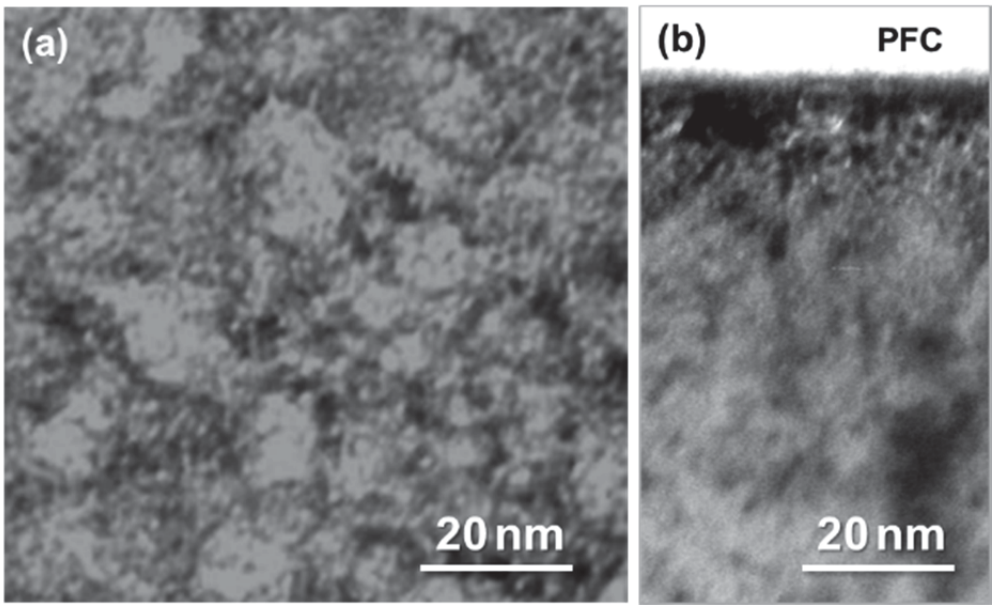

Fig. 3 TEM images of the microstructure formed in 316LSS coupons placed at erosion dominant 9I-3 area in C16 (C16-9I-3-SS). (a) and (b) are top-view of a pre-thinned coupon and cross-sectional view, respectively.

The plasma-facing surface of the coupon C16-9I-4-SS located on the DD area is characterized by dark brown color. Cross-sectional TEM micrographs of C16-9I-4-SS are shown in Fig. 4. The surface is covered by an impurity deposition of about 140 nm in

thickness. Diffuse rings in an electron diffraction pattern (not shown) indicate that it is amorphous. The deposition is not homogeneous; the surface is very rough and a lot of pores up to a few 10 nm in diameter are observed in the matrix. Estimated porosity is 24 vol. %. As can be seen in the magnified picture in Fig. 4 (b), subsurface region of the original 316LSS substrate was highly damaged just as that in the ED area. It seems that this damage was formed by long He glow discharge clearing performed at the beginning of the campaign.

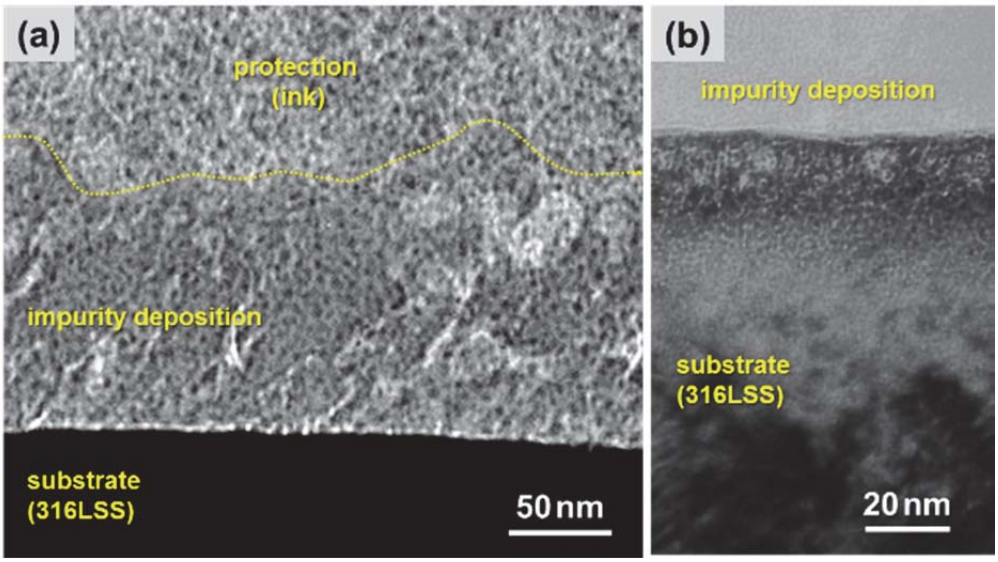

Fig. 4 (a) a cross-sectional TEM image of impurity deposition on 316LSS (C16-9I-4-SS) , and (b) a magnified image showing the interface between substrate and deposition).

3.3 Change in chemical composition

It should be reminded that the W coupons were placed on the inner wall to observe effects of impurity deposition. GD-OES data of W coupons placed at ED area (C16-9I-3-W and C16-9I-5-W) are shown in Fig. 5 (a) and (b), respectively. Working gas and anode diameter for these measurements are Ar and 4 mm, respectively. The sputtering rate of W in the present measurement condition is about 30nm/s. In case of C16-9I-3-W, impurities from the divertor plates (C) and the protection plates (Fe, Cr and Ni) were penetrated into the W substrate and formed mixed material at depths up to 30 nm. Similar mixed layer of about 15 nm in thickness was formed in C16-9I-5-W.

The plasma-facing surface of C16-9I-4-W located at DD area is covered by a thick C dominant layer, as shown in Fig. 5 (c). Content of metallic impurities is very small. XPS analysis indicates that the Fe concentration is about 0.5 at%. Heavily damaged subsurface

region of the W coupon is very clear, namely yields of Fe, Cr and Ni increase locally due to the strong redeposition under the initial glow discharge cleaning.

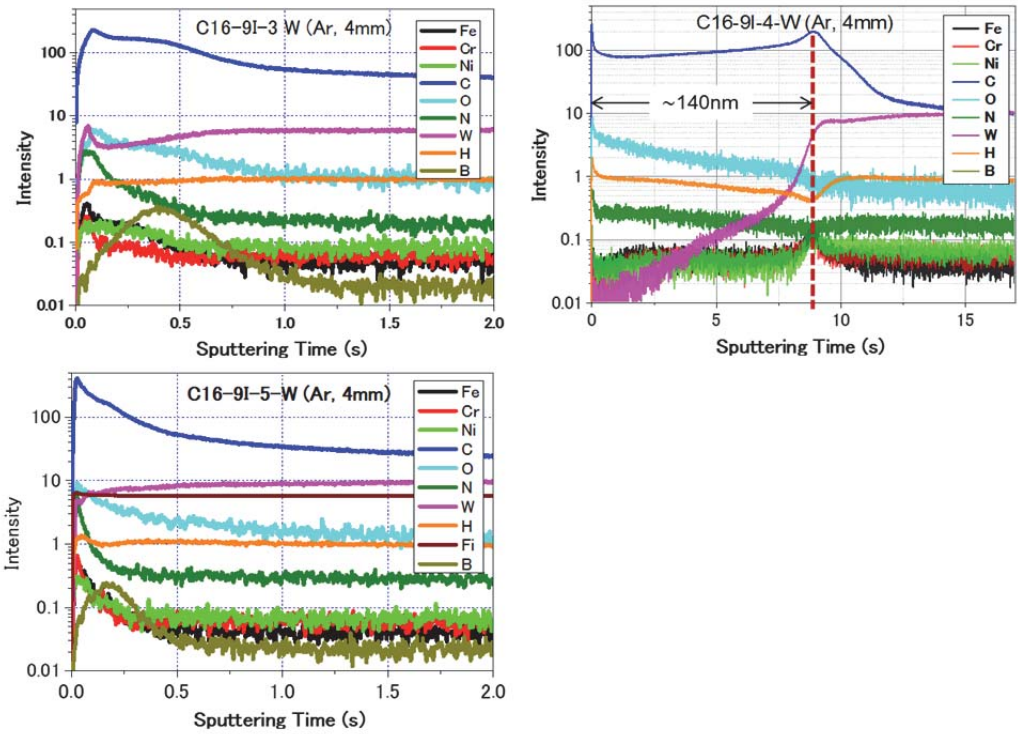

Fig. 5 Results of GD-OES analyses of the W coupons placed on the ED area (a, b) and the DD area (c) and exposed to the LHD plasmas during the campaign C16. In these GD-OES measurements, Ar plasma was used, size of anode was 4 mm in diameter, and the sputtering rate of W was about 30 nm/s.

3.4 Depth profiles of He

Depth profiles of He in 316LSS coupons were examined by means of GD-OES. For this analysis Ne plasma was used to get higher sensitivity for He [12]. Yields of each element in C17-9I-3-SS, C17-9I-4-SS and C17-9I-5-SS are plotted in Fig. 6 against sputtering time. Diameter of the anode used in these measurements is 10mm. Sputtering rate of 316LSS is about 20nm/s.

In case of the ED area (C17-9I-3-SS and C17-9I-5-SS), intensity of He signal increases abruptly up to about 0.3 and then decreases exponentially with increasing sputtering time and keeps constant above 3 s. Judging from the yield assigned to He in the deeper area, where no He exists in actual, background of He signal in 316LSS is 0.075. The background of He signal in W is 0.02 [12] and much lower than that in 316LSS. The rather high background in 316LSS seems to be due to partial overlapping of emission spectrum of He (587.562 nm) with

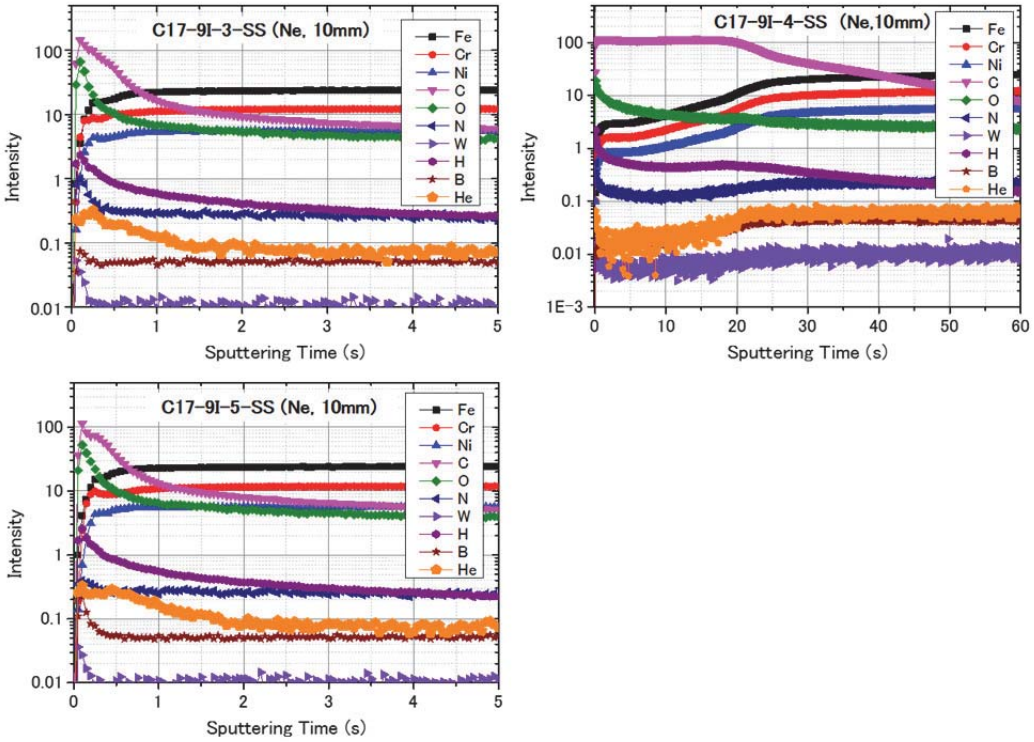

Fig. 6 Results of the GD-OES analyses of the 316LSS coupons placed on the ED area (a, b) and the DD area (c) and exposed to the LHD plasmas during the campaign C17. Ne plasma was used to increase sensitivity in detection of He [12]. Size of anode was 10 mm in diameter, and sputtering rate of 316LSS was about 20 nm/s.

that of a constituent element of 316LSS most likely Cr. These results indicate that He in the plasma-exposed coupons concentrate in the narrow subsurface region of about 60 nm in depth, and the amount of He diverging into the deeper area is little. By subtracting the background, the peak value of He in ED area is about 0.23. Very good agreement between depth distribution of damages and that of He indicates that He are trapped by the radiation-induced defects such as bubbles.

In case of C17-9I-4-SS located on the DD area, on the other hand, signal of He near the top surface is about 0.015 but it increases with increasing sputtering time in proportional to the yield of Cr. It is mentioned above that detection of the He emission is not only due to presence of He itself but also due to presence of Cr. Though it is difficult to detect He at low concentration in the impurity deposition by means of GD-OES, one can say at least that He is not highly concentrated as observed in the ED area.

3.5 Thermal desorption of retained He

Retention and desorption of He in the protection plates are very important to understand

particle recycling in LHD under long-pulse He plasma operation. In the present work, thermal desorption of He from the 316LSS coupons exposed to LHD plasmas (C16-9I-3-SS and C16-9I-4-SS) were measured. In order to understand the repetition effects of plasma discharges, He ions (2keV He^+, 3×10^{21} He^+/m^2) were injected into the C16-9I-4-SS coupon additionally and then TDS spectrum of He was measured. Thermal desorption of He injected into virgin 316LSS [13] were also plotted together for comparison.

Judging from the very defective microstructure (see Fig. 3) and also from the discussion by Bernard et al. on He-plasma irradiation effects in LHD [14], it is expected that not only damage but also He retention in the plasma-exposed coupons have already reached the saturation level. In Fig. 7, TDS spectra of He from the coupons mentioned above are plotted. Ramping rate of the temperature is 1.0 K/s. The amount of desorbed He from each coupons are summarized in table 1. It is notable that the total retention of He in C16-9I-3-SS is 7.5×10^{19} He $/m^2$, which is only 10% of the saturation level with 2 keV He^+ ion irradiation. It looks that short penetration length of He under exposure to the plasmas with much lower average energy and formation of nano-blisters are the possible reasons for the lower retention. The desorption of He from C16-9I-3-SS occurs mainly in the two temperature range, 400–600 K and 900–1200 K. Noticeable differences from the 316LSS coupons irradiated with 2 keV

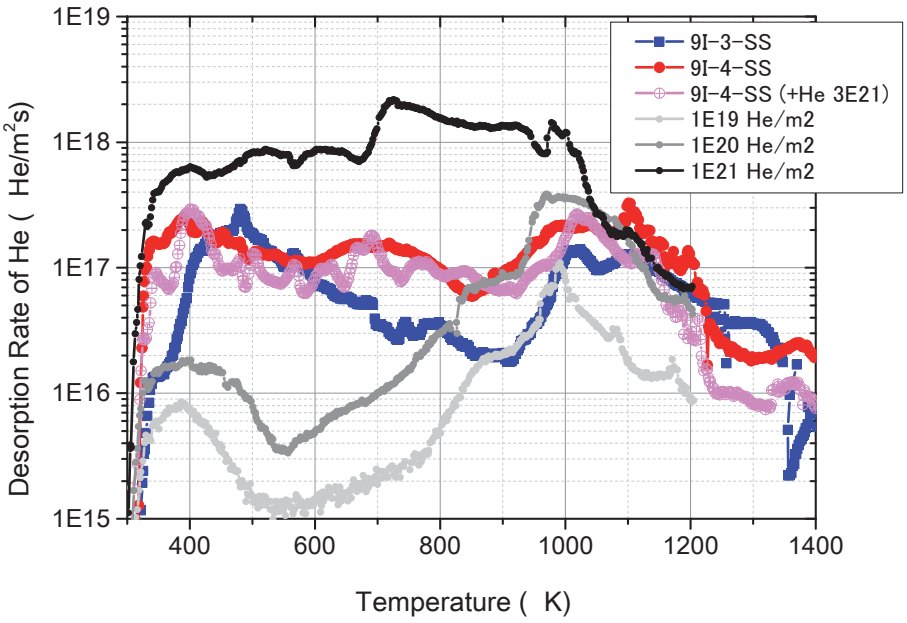

Fig. 7 Thermal desorption of He from 316LSS coupons placed on the ED area (C16-9I-3-SS) and DD area (C16-9I-4-SS) and exposed to the LHD plasma during the campaign C16. Desorption spectra for virgin 316LSS irradiated with 2 keV He^+ ions at 300 K [13] are also plotted for comparison.

Table 1　Amount of desorbed He from each coupons.

Coupons	Total desorption ($1x10^{19}$ He/m^2)	Desorption ≤ 400K ($1x10^{19}$ He/m^2)	Desorption ≤ 450K ($1x10^{19}$ He/m^2)
9I-3-SS	7.5	0.18	0.93
9I-4-SS	14	1.4	2.8
9I-4-SS (+ $3x10^{21}$He$^+$/m^2)	10	0.84	1.8
SS ($1x10^{21}$He$^+$/m^2)	76	3.5	6.4

He^+ ions is the lack of two desorption processes; desorption below 400 K and large continuous desorption up to 900 K. The former indicates that weakly trapped He, which contribute to desorption below 400 K, behave as dynamical retention under the long-pulse He discharges, because the wall temperature is ≤350 K. The weakly trapped He desorbs quickly after finishing the discharge. Judging from the small total retention, number of the trapping sites contributing to the dynamical retention is also much smaller than that estimated from the 2 keV He^+ ion irradiation (3.5×10^{19}/m^2, see table 1). One of the possible mechanisms of the large He desorption up to 900 K observed for the heavily injected 316LSS is the blistering. In case of C16-9I-3-SS, however, nano-blisters have already exfoliated and/or He has already desorbed due to nano-clacking. SEM observation of heating effects on the surface morphology is necessary to confirm the mechanism.

Total retention in the impurity deposited coupon (C16-9I-4-SS) is 1.4×10^{20} He/m^2, which is about two times larger than that for C16-9I-3-SS placed on the ED area. Influence of the additional injection of 2 keV He^+ ions to 3×10^{21} He^+/m^2 on the TDS spectrum is little. This means that the retention of He in the deposition has reached the saturation. It is likely that He was codeposited with C and distribute homogeneously in the deposition having average thickness of 160 nm. The average concentration of He in the amorphous deposition (He/C) is estimated to be about 0.9%. It seems that this value is close to the detection limit of GD-OES. Retained He desorbs constantly between 340 K and 1200 K. It is notable that retention below 400 K is 1.4×10^{19} He/m^2, which is about 9 times larger than that of the ED area coupon (C16-9I-3-SS). These results indicate that thick deposition layers play an important part in the dynamical retention and also additional desorption due to gradual increase of the wall temperature under long-pules operation.

4. Conclusions

Plasma-induced surface modification of 316LSS and its effects on the retention and

desorption of He were examined by exposing many 316LSS and W coupons to the LHD plasma at the inner plasma-facing wall of LHD. The surface modification can be classified into two types as follows: (1) erosion dominant area and (2) deposition dominant area. In the erosion dominant area, subsurface layer of coupon about 20 nm in thickness is damaged heavily by He bombardment under He discharge experiments and glow discharge cleaning with He gas. Extremely dense He bubbles in nano-size and dislocation loops, which induce very strong internal stress, are formed there. Deposited elements such as C and even Fe, Cr and Ni were mixed with substrate elements due to the collision with energetic particles from the plasma. In the deposition dominant area, wide area of the inner wall was colored by the deposition of carbon dominant materials. Content of metallic impurities is only about 0.5 at%. Its structure is amorphous and porous.

Retention of He in the erosion dominant area is saturated at 7.5×10^{19} He /m^2. Most of them are trapped strongly by the He bubbles formed in the 316LSS substrate. Weakly trapped He, which can desorb below 400 K, does not remain because the surface temperature under the discharge is ≤350 K. It is considered that these He play roles in the dynamical retention.

Retention of He in the C-rich deposition is also saturated. It seems that they are gradually codeposited with C as much as possible under He discharges. Average concentration of He, He/C, is about 0.9%. The retained He desorbs almost constantly between 340 K and 1200 K. This indicates that thick deposition layers play an important part in the dynamical retention and also additional desorption due to gradual increase of the wall temperature under long-pule discharges.

References

[1] T. Mutoh et al., Nucl. Fusion 47 (2007) 1250–1257.
[2] M. Tokitani et al., J. Nucl. Mater. 417 (2011) 668–672.
[3] H. Zushi et al., Nuclear Fusion 43 (2003) 1600–1609.
[4] M. Sakamoto et al., Nucl. Fusion 42 (2002) 165–168.
[5] H. Zushi, et al., J. Plasma and Fusion Research, 79 (2003) 1302-1316.
[6] M. Tokitani et al., Fusion Sci. Technol. 58(2010) 305–320.
[7] M. Tokitani et al., J. Nucl. Mater. 438 (2013) S818–S821.
[8] M. Tokitani et al., J. Nucl. Mater. 463 (2015) 91–98.
[9] H. Iwakiri et al., J. Nucl. Mater. 283–287 (2000) 1134.
[10] N. Yoshida et al., I. Nucl. Mater. 258–263 (1998) 173.

[11] M. Tokitani et al., J. Nucl. Mater. 386–388 (2009) 173–176.

[12] Y. Hatano et al., Fusion Eng. Des. 87 (2012) 1091–1094.

[13] M. Tokitani et al., J. Nucl. Mater. 329–333 (2004) 761–765.

[14] E. Bernard et al., J. Nucl. Mater. 463 (2015) 316.